Microscopic models for time-resolved photoluminescence in α-PTCDA single crystals

R Scholz, A Yu Kobitski, I Vragović, T U Kampen, D R T Zahn
Institut für Physik, Technische Universität Chemnitz, Germany

Wagner H P
Department of Physics, University of Cincinnati, USA

Abstract. In the present work, we analyse the radiative and non-radiative recombination channels in α-PTCDA (3,4,9,10 perylene tetracarboxylic dianhydride) by applying time-resolved photoluminescence (PL) techniques in the 100 ns range between temperatures of $T = 11$ K and $T = 300$ K. These experimental findings are interpreted with microscopic calculations of the dispersion of Frenkel excitons and the investigation of different dimer geometries using time-dependent density functional theory. Based on the latter approach, we can identify radiative recombination from excimer states and from anion-cation pairs. From the temperature dependence of the different PL channels we gain some insight into radiative lifetimes and the energy barriers for non-radiative de-excitation.

1. Introduction

Among the molecular semiconductors, some substances like Alq_3 show a remarkably high photoluminescence (PL) efficiency and are therefore well suited for organic light emitting diodes, while many layered crystalline materials like thiophenes or perylene derivatives are poor emitters [1, 2]. The PL efficiency can be increased by adding functional groups reducing the aromaticity of the molecules [3, 4]. For both classes of organic substances, such functionalizations result in deviations from the planarity of the molecules and in a larger distance between different molecular sites. As a consequence, the inter-molecular interactions are reduced, and the corresponding PL quenching mechanisms become less efficient.

On the other hand, crystals of planar molecules are interesting model systems for studying the influence of the inter-molecular interactions on the PL spectra. In the case of crystalline PTCDA, the stacking distance is much shorter than in the crystalline phases of other perylene derivatives, so that this substance is particularly suited for such investigations. Previous time-resolved PL studies of PTCDA and MePTCDI samples have revealed PL decay times times of about 4 ns in the case of dissolved monomers and amorphous samples [5, 6], while poly-crystalline PTCDA films of sufficient thickness show a radiative lifetime of about 11 ns at low temperatures [7, 8].

In the present work, we extend these investigations to the temperature dependence of time-resolved PL measured on single crystals of α-PTCDA [9, 10]. Our results are interpreted with microscopic calculations based on the transfer of Frenkel excitons [11, 12] and with the investigation of different dimer geometries using time-dependent density functional theory (TD-DFT) [13], together with models for activated non-radiative decay.

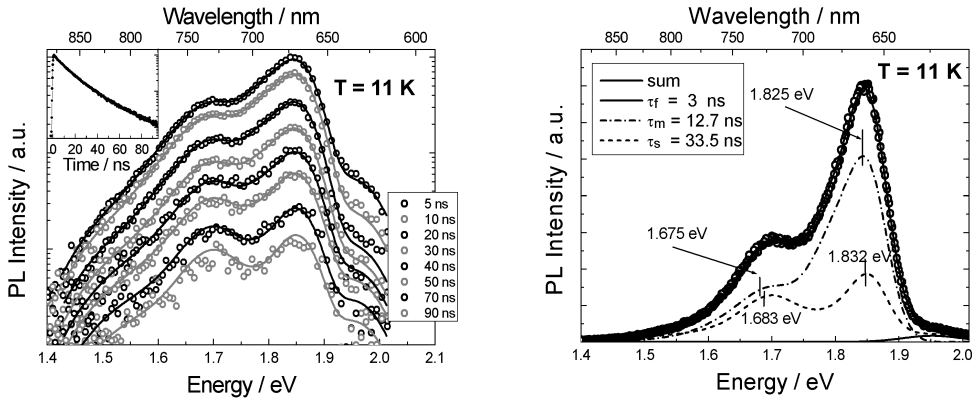

Figure 1. Left: Low-temperature ($T = 11$ K) PL spectra measured at different delays after the excitation pulse ($\circ$) together with curves based on a model of three PL channels with decay times of $\tau = (3 \pm 1)$ ns, (12.7 ± 0.4) ns (Frenkel exciton), and (33.5 ± 4) ns (CT exciton). In the inset, the semi-logarithmic scale of the spectrally integrated PL reveals a clear non-exponential time dependence. Right: PL spectra integrated over a delay window from -5 ns to 95 ns, with a decomposition into the lineshapes of the three PL channels: Frenkel exciton (dash-dotted), CT exciton (dashed), fast decaying PL channel around 1.95 eV (solid), and sum of all components (solid line superimposed to experimental data points ($\circ$) [9].

2. Experimental

The α-PTCDA crystallites used in the present investigation were grown by double sublimation in high vacuum. For the time-resolved PL measurements the PTCDA crystals were excited with a pulsed dye laser synchronously pumped by a mode-locked Ar^+ ion laser, resulting in 20 ps pulses at an energy of 2.19 eV (565 nm) focused to a spot of about 250 μm on the sample. As the repetition rate of 80 MHz defined by the cavity length of the ion laser exceeds the decay rate of the slowest PL components, it was reduced to 4 MHz using a cavity dumper. The time-resolved PL was analysed using a CROMEX 250IS imaging spectrograph and detected by a Hamamatsu C4334 Streakscope with a time resolution better than 50 ps. In order to protect the streakscope against stray light from the laser, a filter with a cutoff at 590 nm (2.10 eV) was used. In the range 1.5 - 2.1 eV investigated in the present work, the flatness of the spectral response of the entire measuring system was checked with black body radiation from a tungsten lamp with known emission spectrum, and therefore no spectral correction was applied to the subsequent PL measurements. For the low temperature ($T = 11$ - 300 K) measurements, a closed-cycle He cryostat CTI-Cryogenics was used.

3. Time-resolved PL spectra at low temperature

At the lowest temperature of about $T = 11$ K, we found clear evidence for three distinct PL channels with decay times of (3 ± 1) ns, (12.7 ± 0.4) ns, and (33.5 ± 4) ns, cp. Fig. 1 [9]. For the PL intensity integrated over the delay window of -5 ns to 95 ns after the excitation pulse, the two slower decay rates contain a vibronic progression of three subbands near 1.83 eV, 1.68 eV and 1.52 eV, whereas the fastest PL channel consists of a single structure around 1.95 eV. The dominating PL band decaying within about 13 ns can be modeled quantitatively as recombination out of an indirect minimum of the Frenkel exciton dispersion discussed in Sec. 5. From the dimer calculations in Sec. 6 we assign the slowest PL band to recombination resulting from charge transfer (CT) between a pair of an anionic and a cationic molecule. Based on the decay dynamics of this PL band at higher temperatures, three contributions

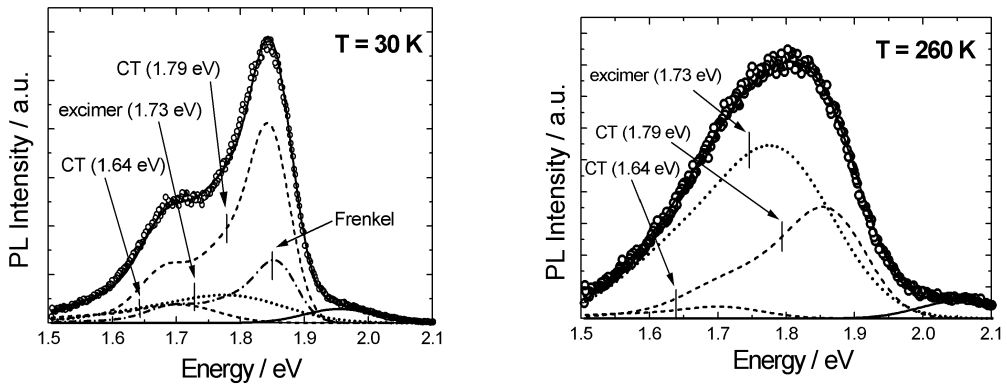

Figure 2. Contributions to the experimental PL spectra integrated over a delay window of -5 ns to 45 ns ($\circ$) , for $T = 30$ K (left) and $T = 260$ K (right): Frenkel exciton with maximum around 1.84 eV (dash-dotted), excimer with $\langle E_{\rm PL}\rangle = 1.73$ (dotted), low-energy CT band around $\langle E_{\rm PL}\rangle = 1.64$ eV (dashed), high-energy CT band with $\langle E_{\rm PL}\rangle = 1.79$ eV (dashed), and high-energy satellite around 1.95 eV at $T = 30$ K and around 2.05 eV at $T = 260$ K (solid), and sum of all contributions (solid line). The broadenings of all the recombination channels increase with temperature.

arising from different arrangements of the two molecules involved can be distinguished: First a stack of a positively and a negatively charged molecule results in a PL band with $\langle E_{\rm PL}\rangle = 1.64$ eV, second an ion pair involving the two different molecules in the crystal unit cell is responsible for the largest feature around 1.83 eV and vibrational satellites at lower energy, and third a further dimer geometry contributes to the slow decay of the high-energy peak at 1.95 eV. The fastest decay channel around 1.95 eV is attributed to an excimer geometry with rather low radiative decay rate, but a fast non-radiative decay into more favourable dimer geometries, especially the stacked ion pair whose PL intensity rises up to a delay of about 3 ns after the excitation pulse.

4. Time-resolved PL as a function of temperature

At higher temperatures, a new PL channel opens up, becoming the predominant PL band above $T = 220$ K, cp. Figs. 2 and 3. It can be interpreted as an excimer consisting of two stack neighbours, as will be discussed in Sec. 6 in more detail. Furthermore, the high-energy satellite around 1.95 eV is quenched above $T = 150$ K, and instead a different PL band near 2.05 eV develops. Based on the Frenkel exciton model discussed in the next Sec., this high-energy feature can be assigned to a relaxed excited monomer.

The temperature-dependent decay times τ of each of the PL channels can be modeled as a superposition of a radiative rate and activated non-radiative decay:

$$\frac{1}{\tau} = \gamma = \gamma_{\rm rad} + \gamma_{\rm non-rad} \exp\left[\frac{-E_{\rm act}}{k_B T}\right], \tag{1}$$

where $\gamma_{\rm rad} = \tau_{\rm rad}^{-1}$ is the inverse of the radiative lifetime, $\gamma_{\rm non-rad}$ a non-radiative recombination rate, and $E_{\rm act}$ the corresponding activation barrier. The PL efficiency of the different PL channels can be expressed as

$$\eta = \frac{\gamma_{\rm rad}}{\gamma}, \tag{2}$$

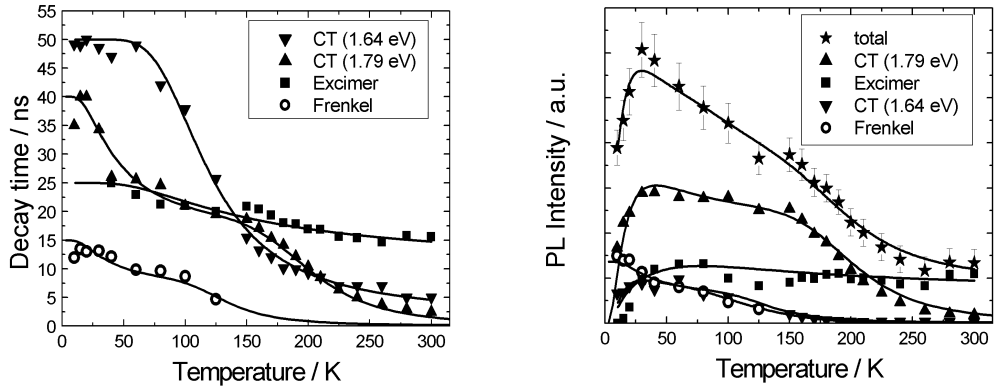

Figure 3. Left: Lifetimes of the different PL bands, where the model curves according to eq. (1) are calculated with $\tau_{\rm rad} = 15$ ns for the Frenkel excitons, 40 ns for the high-energy CT band around $\langle E_{\rm PL}\rangle = 1.79$ eV assigned to an anionic and a cationic molecule of different orientations, 50 ns for the low-energy CT band around $\langle E_{\rm PL}\rangle = 1.64$ eV assigned to an anion-cation stack, and 25 ns for the PL arising from the stacked excimer. The barriers for non-radiative decay are $E_{\rm act} = 6$ meV and 88 meV for the Frenkel excitons, two barriers of 6 meV and 135 meV for the high-energy CT band, 42 meV for the low-energy CT band, and 30 meV for the excimer. Right: Temperature-dependent intensities of the different PL bands, with model curves based on the efficiencies η and densities n according to eqs. (1-3) and formation barriers of $E_{\rm form} = 1.5$ meV for the high-energy CT band, 1.4 meV for the excimer, and 6 meV for the low-energy CT band.

so that the temperature dependence of the PL lifetimes and intensities can be treated on the same footing, cp. Fig. 3. For simplicity the lifetime obtained for the lowest temperature is interpreted as the radiative lifetime of each PL band, even though non-radiative de-excitation channels might contribute even in this temperature regime, especially for the slowest recombination channels. Some PL channels involve a barrier for the formation of the precursor state, so that the density of these states is assumed to depend on the temperature as

$$n(T) = n_0 \exp\left[\frac{-E_{\rm form}}{k_B T}\right], \tag{3}$$

resulting in an increase of the corresponding PL intensities between $T = 11$ K and about $T = 50$ K.

For the high-energy CT band, two non-radiative de-excitations can be distinguished, involving barriers of $E_{\rm act} = 6$ meV and 135 meV, respectively. We suppose that the decay over the lower barrier results again in an emissive CT state, while the decay over the higher barrier leads to the quenching of this PL band above $T = 150$ K. Within the error margins of our model analysis, the formation barrier $E_{\rm form} = 6$ meV for the low-energy CT band coincides with the lower of the two activation barrier for non-radiative decay of the high-energy CT band, so that it is tempting to assign the former to the final state after non-radiative decay of the latter. Albeit this decay route seems reasonable due to the microscopic dimer models discussed in Sec. 6, the similarity of the formation and decay barriers could be a pure coincidence.

5. PL from Frenkel excitons

Based on a model including the transfer of Frenkel excitons, we can calculate the frequency-dependence of the anisotropic dielectric tensor [11], cp. the schematic optical cycle in Fig.

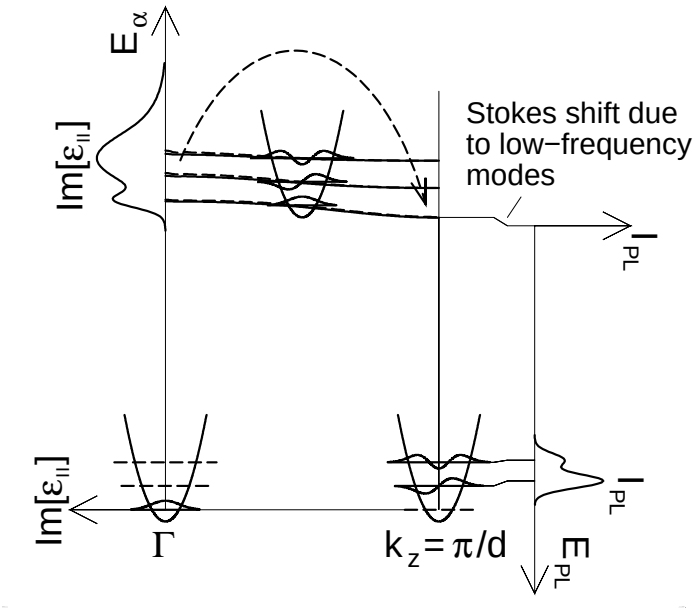

Figure 4. Schematic optical cycle in the microscopic model based on the elongation of an effective internal vibration and the transfer of Frenkel excitons between different molecules. After the absorption at Γ, the exciton relaxes towards the dispersion minimum at the surface of the Brillouin zone (dashed arrow). At any finite wave vector, the lowest vibrational level in the electronic ground state is not available as the final state after a vertical transition downwards. Vibrational sublevels not involved in the vertical excitation and de-excitation are indicated as dashed lines.

4, where the linear response at Γ is visualized with an average of its diagonal components. The model ingredients are the elongation of an effective internal vibration at $\hbar\omega_{\text{eff}} = 0.17$ eV together with the transfer of Frenkel excitons arising from the interaction between the transition dipole moments on different molecular sites. At all temperatures, the optical excitation starts in the vibrational ground state because the energy of the effective internal mode is far above the thermal energy. The generalization of this approach to the **k**-space dispersion of the Frenkel excitons results in a minimum at the surface of the Brillouin zone [12], an obvious candidate for a red-shifted PL band. As the vibrational ground state has vanishing total momentum, it is not available as a final state after vertical de-excitation of this lowest Frenkel exciton state, resulting in a further decrease of the PL energy by one vibrational energy quantum $\hbar\omega_{\text{eff}}$. The small energy shifts of the final states after recombination with respect to the higher harmonics of the effective vibrational mode result from a correlation between these vibrational sublevels. Like in absorption, it arises again from the transfer of the Frenkel excitons. A small contribution to the total Stokes shift results from the low-frequency internal and external vibrational modes not included in the Frenkel exciton model. This part of the PL red-shift is in the range expected from the elongations of the corresponding vibrational modes determined with resonant Raman techniques [12, 14, 15].

From the density of states of the Frenkel exciton dispersion, we can calculate a temperature-dependence of the position of the resulting PL band, in good agreement with the experimental findings of $\partial E_{\text{PL}}/\partial T \approx 5 \times 10^{-2}$ meV/K.

The high-energy satellite around 2.05 eV can be obtained from an average of the lowest exciton band $\langle E_{00}(\mathbf{k})\rangle = 2.16$ eV corrected by a Stokes shift of -0.11 eV expected from low-frequency internal and external vibrational modes [12].

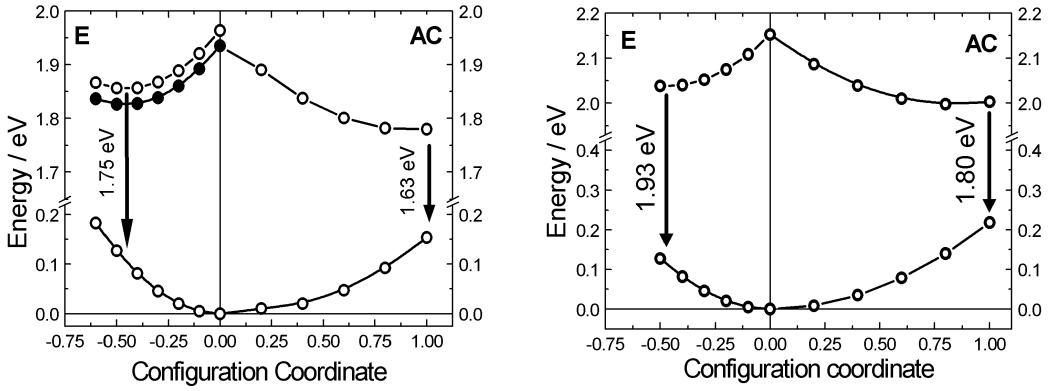

Figure 5. Left: Configuration coordinate diagram of a stack dimer, where the deformation of the excimer towards the left is compatible with the relaxed excited state of the monomer, and the deformation towards the right with an anion-cation (AC) pair. For the excimer (E), the higher transiton at 1.75 eV is dipole-allowed, while the lower transition is forbidden by parity. Right: Configuration coordinate diagram for a pair of non-coplanar molecules of different orientation, with a distance of 10.5 Å between their centers of mass.

6. PL from relaxed dimer geometries

All calculations discussed in the present Sec. have been performed with the TD-DFT scheme based on the B3LYP functional as implemented in the GAUSSIAN98 package. The choice of the relatively small 3-21G basis set was motivated by the need to apply precisely the same approach both to PTCDA monomers and dimers. For the dimers this was the largest possible basis set which could be run on the HP-9000 N4000 hardware used, and each dimer geometry took about 40 - 48 hours on a single processor of this system, resulting in a total CPU time of about 4 months for all the 65 dimer geometries investigated.

The model geometries are based on the atomic positions in the crystal unit cell determined by X-ray diffraction [16], where the positions of the hydrogen atoms have been readjusted with a calculation of the 3-dim unit cell applying density functional tight-binding (DFTB) techniques [17]. After reference calculations for the corresponding monomers and dimers in geometries compatible with the so-defined α-PTCDA crystal, the molecular geometries have been modified as in the relaxed excited state of the monomer and in anionic and cationic molecules, as discussed earlier in the interpretation of resonant Raman spectra of PTCDA [15] and TD-DFT calculations for stacked dimers [12]. Two kinds of deformed dimers have been investigated: Anion-cation pairs and excimer states, where the molecules are deformed as in the relaxed excited state of the monomer. In both cases, the prefactor of the overall deformation has been varied in 20 % steps between the crystal reference geometry and the largest deformation applied, corresponding to the ionic geometry for the anion-cation pairs and to half of the deformation in the relaxed excited state for each molecule in the pair forming the excimer. In the latter case, it turned out that the minimum of the excimer energy occurs around 45 % of the deformation of the relaxed excited monomer.

The previous TD-DFT calculations for a stack dimer compatible with the crystal geometry and the corresponding anion-cation pair [12] have been extended to dimers consisting of two identical molecules displaced by the lattice vector **b**, and to dimers involving the two different basis molecules in the unit cell. In the latter case, nearly coplanar geometries and molecule pairs distributed over two consecutive PTCDA layers have been investigated. In each case, we have performed a careful adjustment of the overall energy scale due to the lack of the crystal surroundings.

In Fig 5, we report two typical configuration coordinate diagrams for molecular dimers: The stack geometry, and a dimer consisting of two inequivalent molecules extended over two consecutive molecular planes in the crystal. From the minima of the excited states in the stack geometries investigated, we assign the observed low-energy CT band with $\langle E_{\mathrm{PL}} \rangle = 1.64$ eV to the transition energy of 1.63 eV in the anion-cation stack, while the excimer PL band with $\langle E_{\mathrm{PL}} \rangle = 1.73$ eV dominating at high temperatures can be related to the transition energy of 1.75 eV for an excimer in a stacked geometry. The fact that the lowest transition in the stacked excimer is parity-forbidden could be responsible for the low PL efficiency of crystalline PTCDA. From the calculations of the dimer involving the two different non-coplanar basis molecules, we assign the observed average of $\langle E_{\mathrm{PL}} \rangle = 1.79$ eV to the CT recombination between the two ions at 1.80 eV in the configuration coordinate diagram. The energetic minimum in the excimer geometry determines a transition energy of 1.93 eV, a candidate for the slow component of the high-energy satellite in the low-temperature PL spectra.

The agreement between these microscopic TD-DFT calculations for various dimer geometries with the positions of the observed PL bands is quite remarkable. As our approach does not account for a contribution of the external phonon modes to the Stokes shift [12, 14], we can use this deficiency for an estimate of systematic errors of the TD-DFT calculation. From their resonant Raman intensities, we expect these modes to contribute 40 meV to the reorganization energy in absorption [12]. Even though the contribution of the external phonons to the Stokes shift of a transition localized on a dimer is unclear, we can use this reorganization energy in absorption for an estimate of 80 meV for the Stokes shift, defining an upper limit for possible systematic deviations of the TD-DFT results.

7. Conclusion

As a conclusion, we have applied time-dependent PL techniques to α-PTCDA single crystals in a temperature range of $T = 11$ to 300 K. From microscopic calculations based on the transfer of Frenkel excitons and TD-DFT calculations for molecular dimers, we were able to assign the energetic positions of all the observed PL bands. Furthermore, the calculated radiative lifetime of the Frenkel excitons is in good agreement with the PL decay channel dominating at low temperature. Models for activated formation and non-radiative decay of the precursor states of the different PL bands allowed us to propose decay routes connecting these low-lying excited states.

References

[1] Muccini M, Lunedei E, Taliani C, Beljonne D, Cornil J, and Brédas J L, 1998 J. Chem. Phys. **109**, 10513-20
[2] Nollau A, Hoffmann M, Floreck K, Fritz T, and Leo K, 2000 J. Appl Phys. **87** 7802-4
[3] Gigli G, Barbarella G, Favaretto L, Cacialli F, and Cingolani R, 1991 Appl. Phys. Lett. **75**, 439-41
[4] Schlettwein D, Graaf H, Michaelis W, Jaeger N, Unold T, Bauer G H, Yanagi H, 2001 Proc. of the SPIE **4456** 48-56
[5] Bulović V, Burrows P E, Forrest S R, Cronin J A, and Thompson M E, 1996 Chem. Phys. **210** 1-12
[6] Gómez U, Leonhardt U M, Port H, and Wolf H C, 1997 Chem. Phys. Lett. **268**, 1-6
[7] So F F and Forrest S R, Phys. Rev. Lett. 1991 **66** 2649-52
[8] Forrest S R, 1997 Chem. Rev. **97** 1793-1896
[9] Kobitiski A Yu, Scholz R, Vragović I, Wagner H P, and Zahn D R T, 2002 Phys. Rev. B accepted
[10] Kobitiski A Yu, Scholz R, Salvan G, Kampen T U, Wagner H P, and Zahn D R T, 2002 Appl. Surf. Sci. in press
[11] Vragović I, Scholz R, and Schreiber M, 2002 Europhys. Lett. **57** 288-94
[12] Scholz R, Vragović I, Kobitski A Yu, Salvan G, Kampen T U, Schreiber M, and Zahn D R T,, 2002 in: Proc. of Int. School of Physics "E. Fermi", course CXLIX: Organic nanostructures: Science and applications, IOS Press Amsterdam in press
[13] Stratmann R E, Scuseria G E, Frisch J F, 1998 J. Chem. Phys. **109**, 8218-24

[14] Salvan G, Tenne D A, Das A, Kampen T U, and Zahn D R T, 2000 Organic Electronics **1** 49-56
[15] Scholz R, Kobitski A Yu, Kampen T U, Schreiber M, Zahn D R T, Jungnickel G, Elstner M, Sternberg M, T. Frauenheim T, 2000 Phys. Rev. B **61** 13659-69
[16] Lovinger A J, Forrest S R , Kaplan M L , Schmidt P H , and Venkatesan T, 1984 J. Appl. Phys. **55** 476-82, and private communication
[17] Frauenheim T, Seifert G, Elstner M, Hajnal Z, Jungnickel G, Porezag D, Suhai S, and Scholz R, 2000 phys. stat. sol. (b) **217** 41-62